Materials Today Bio 23 (2023) 100795

Contents lists available at ScienceDirect

Materials Today Bio

journal homepage: www.journals.elsevier.com/materials-today-bio

Chondrocyte targeting gold nanoparticles protect growth plate against inflammatory damage by maintaining cartilage balance

Xue Bai [a,d,1], Hongyan Sun [b,1], Lina Jia [b], Junjie Xu [b], Peng Zhang [b], Deyuan Zhang [b,c], Yu Gu [a,d,*], Bo Chen [b,**], Lin Feng [b,c,***]

[a] School of Biomedical Engineering, Capital Medical University, Beijing, 100069, China
[b] School of Mechanical Engineering & Automation, Beihang University, Beijing, 100191, China
[c] Beijing Advanced Innovation Center for Biomedical Engineering, Beihang University, Beijing, 100083, China
[d] Beijing Key Laboratory of Basic Research in Clinical Applied Biomechanics, China

ARTICLE INFO

Keywords:
Extracellular matrix
Gold nanoparticles
Growth plate
Inflammation-induced cartilage damage

ABSTRACT

Cartilage destruction caused by inflammation is a clinical challenge. Many studies have investigated cartilage destruction in adults, but little research was conducted on children. In this study, the protective effect of gold nanoparticles (AuNPs) on the cartilage of children was realized by counteracting chondrocyte apoptosis and extracellular matrix (ECM) degradation in a young mouse model of lipopolysaccharide (LPS)-induced growth plate (GP) cartilage damage. Initially, engineered AuNPs can be efficiently absorbed by chondrocytes, approximately 20 times the amount absorbed by macrophages, resulting in a 29% ± 0.05% increase in chondrocyte viability. Then, AuNPs exposure significantly reduced the release of inflammatory cytokines and secretion of ECM degradation factors induced by LPS. Subsequently, AuNPs were applied to resist LPS-induced cartilage destruction in young mice. AuNPs inhibited the formation of gaps, without chondrocytes and extracellular matrix, between the proliferative and hypertrophy zones of the GP cartilage, and the gaps were noticeable in the LPS group. This finding can be attributed to the capability of AuNPs to reduce the LPS-induced apoptosis rate of mouse chondrocytes by 72.38% and the LPS-induced ECM degradation rate by 70.89%. Further analysis demonstrated that remission is partly due to AuNPs' role in maintaining the balance of catabolic and anabolic factors in the ECM. Altogether, these findings indicate that AuNPs can partially protect the cartilage of children from inflammatory damage by suppressing chondrocyte apoptosis and ECM degradation.

1. Introduction

Cartilage is a specialized dense connective tissue that is only composed of chondrocytes and cartilage matrix, it does not contain blood vessels, nerves, and lymphatic connective tissue, and it has a poor self-repair ability [1–3]. Cartilage does not regenerate spontaneously when it gradually diminishes as a result of aging or when it is damaged by exercise or disease [4] because of the minimal cartilage collagen turnover [5,6]. In recent decades, the treatments of cartilage regeneration, such as implantation of stem cells [7] or autologous chondrocytes [8] via scaffolds [9], cell vesicle injections [10], or electrical stimulation [11], have significantly advanced [12]. Encouragingly, researchers have identified stem cells [13,14] or proteins [15] in cartilage tissues that have demonstrated potential for cartilage regeneration. However, cartilage lesions are often asymptomatic [16,17]; thus, the prevention of cartilage injury based on age, obesity, occupational injury, or trauma

Abbreviations: AuNPs, Gold Nanoparticles; ECM, Extracellular Matrix; LPS, Lipopolysaccharide; GP, Growth Plate; RZ, Resting Zone; PZ, Proliferative Zone; HZ, Hypertrophic Zone; MMPs, Matrix Metalloproteinases; MUA, 11-mercaptoundecanoic acid; CCK-8, Cell Counting Kit-8; PI, propidium iodide; TUNEL, TdT-mediated dUTP nick-end labeling; IL-1β, Interleukin 1β; TNF-α, Tumor Necrosis Factor-α; ELISA, Enzyme-linked Immunosorbent Assay; CCL-2, Chemokines-2; EO, Endochondral Ossification; CF, Cystic Fibrosis.

* Corresponding author. School of Biomedical Engineering, Capital Medical University, Beijing, 100069, China.
** Corresponding author.
*** Corresponding author. School of Mechanical Engineering & Automation, Beihang University, Beijing, 100191, China.
E-mail addresses: xuebai@ccmu.edu.cn (X. Bai), ygu@ccmu.edu.cn (Y. Gu), chen_bo1991@163.com (B. Chen), linfeng@buaa.edu.cn (L. Feng).
[1] These authors contributed equally.

https://doi.org/10.1016/j.mtbio.2023.100795
Received 7 June 2023; Received in revised form 9 August 2023; Accepted 11 September 2023
Available online 14 September 2023

has become a clinical goal [18,19].

A major pathological feature of these cartilage defects is the inflammation-induced degradation of the cartilage matrix [20] or chondrocyte apoptosis [21], a process that can occur at all life stages. In adults, inflammation-induced cartilage defects have been reported in osteoarthritis [22], exfoliative osteochondroitis [23], osteonecrosis, and osteochondral fractures [24], and results of numerous studies have helped advance the prevention, diagnosis, and treatment. During growth and development, children may experience local or systemic inflammation caused by various disorders such as Crohn's disease [25], rheumatoid arthritis [26], colitis [27], inflammatory bowel disease [28], and other chronic inflammatory diseases [29]. Inevitably, such inflammations damage the cartilage, including the growth plate (GP) cartilage which is characteristic of childhood [30]. GP damage can lead to severe complications, such as fractures, deformities, impaired longitudinal growth, or permanent stunting [31–33]. Thus, establishing therapeutic strategies to prevent inflammatory damage to the GP in children is a necessary measure to ensure the healthy growth of children.

GP is a differentiated, rapidly growing cartilaginous structure that exists only in childhood and can be converted into bones [34]. GP chondrocytes are arranged in columnar order and can be divided into the resting zone (RZ), proliferative zone (PZ), and hypertrophic zone (HZ) from the epiphysis to the diaphysis according to cell morphology and physiological function [35]. PZ chondrocytes are different from RZ chondrocytes. They can divide and proliferate continuously and secrete extracellular matrix (ECM) mainly composed of type II collagen and proteoglycans [36]. Subsequently, PZ chondrocytes are gradually differentiated into hypertrophic chondrocytes and formed the HZ. HZ chondrocytes induce the secretion of matrix metalloproteinases (MMPs) and promote the degradation of the cartilage matrix, including collagens and proteoglycans [37]. Finally, HZ chondrocytes slowly undergo apoptosis, degradation, and mineralization in the cartilage matrix, followed by the invasion of blood vessels and osteoclasts, and finally, matrix ossification around the cells, leading to bone formation [30]. A correct and strict sequence of chondrocyte function is essential to ensure normal osteogenic growth.

In our previous study using a lipopolysaccharide (LPS)-induced bone erosion model of 5-week-sized BALB/c mice, not only did the model mice develop an osteoporotic phenotype [38], but also a GP cartilage vacancy (absence of chondrocytes and ECM) resulted in separation at the PZ and HZ junction. This phenomenon was not observed in the control group or the gold nanoparticle (AuNP)-treated group. In this study, we demonstrated that AuNPs can protect the GP of the cartilage of young mice from inflammation by blocking inflammation-induced chondrocyte apoptosis and ECM degradation.

2. Materials and methods

2.1. Synthesis of AuNPs

AuNPs were fabricated from chloroauric acid (HAuCl4) reduced by sodium citrate as previously described [38,39]. In detail, 1% HAuCl4 was diluted 100 times with deionized water (ddH_2O) and heated to a boil at pH 3.42–3.46. Then, 5% sodium citrate was added. The volume ratio to the HAuCl4 solution was 1:2. The solution was heated until it turned wine red and there was no color change anymore. The solution was cooled at room temperature and centrifuged at 7000 g for 20 min, the supernatant was discarded, and the sediment was dissolved in ddH_2O. Next, 0.5 mg of the citrate–AuNP solution was diluted in 20 mL of reaction solution (0.05% Tween 20 and 0.25 mM Na–citrate solution), and pH was adjusted to 10–11 before argon aeration for 5 min to clear the air. Thereafter, 250 μL of 4 mM 11-mercaptoundecanoic acid (MUA) was added and stirred for 16–18 h in a sealed tube. The sediment was dissolved in ddH_2O after being centrifuged at 10,000 g for 20 min.

2.2. Characterization of AuNPs

Ultraviolet and visible spectrophotometer (UV–Vis, PERSEE, China) was used to determine the surface plasma resonance absorption spectrum of AuNPs. High-resolution transmission electron microscopy (TEM, JEOL2000, JEOL Ltd., Japan) was performed to determine the morphology and structure of AuNPs based on the image of electron diffraction. Dynamic laser scattering (Nicomp TM 380/ZLS, USA) was used to measure the hydrodynamic diameter and zeta potential in the water. The surface composition of AuNPs was determined by X-ray photoelectron spectroscopy (Thermo Fisher Scientific, Waltham, MA, USA).

2.3. Cell culture

Leukemia cells of mouse mononuclear macrophage (Raw 264.7) are purchased from the National Laboratory Cell Resource Sharing Platform. Primary chondrocytes were obtained from the tibial plateau cartilage of 5-week-old female BALB/c mice. Both of them were cultured with Dulbecco's minimum essential medium (which contains 4500 mg/L D-glucose) supplemented with 10% fetal bovine serum and 1% penicillin–streptomycin solution (HyClone, Logan, UT, USA) in a humidified atmosphere of 5% CO_2 at 37 °C.

2.4. Cytotoxic test of AuNP

Cytotoxicity of AuNPs was determined based on cell viability and apoptosis using Cell Counting Kit-8 (CCK-8), calcein–AM/propidium iodide (PI) staining kit, and annexin V–fluorescein isothiocyanate (FITC)/PI kit (Dojindo Laboratories, Japan). Raw 264.7 and primary chondrocytes were exposed to AuNPs at a concentration of 3 μg/mL for 24 h. Then, the treated cells were co-cultured in the medium with 10% CCK-8 solution for 20 min, and the absorbance was measured at a wavelength of 450 nm using a microplate reader (Molecular Devices, LLC, CA, USA). Treated cells were co-cultured in a medium with 2 μM calcein–AM/PI solution for 20 min. Then, cells were washed three times with sterilized phosphate-buffered saline (PBS), and images were captured by laser confocal fluorescence microscopy (Nikon A1, Japan). Treated cells were stained with PI/annexin V–FITC for 15 min, and the apoptosis ratio was measured by flow cytometry (Bio-Rad Laboratories, Hercules, CA, USA). Treated cells were stained with toluidine blue (Solarbio Life Science & Technology Co., Ltd., Beijing, China).

2.5. LPS-induced GP cartilage injured in mice

BALB/c mice (5 weeks old, female, 15 ± 1.2 g) were bought from Beijing Huafukang Bioscience Co., Inc., and fed adaptively for 1 week. Then, the mice were divided into four groups randomly: no treatment (control group), treated with LPS alone (LPS group), treated with AuNP alone (AuNP group), and treated with both LPS and AuNPs (LPS + AuNP group). The four groups were intraperitoneally injected with normal saline (0.9% NaCl), AuNPs (40 mg/kg), LPS (5 mg/kg), and LPS + AuNPs, respectively. Injections were given every 3 days for 15 days. On day 16, all mice were anesthetized with 2% pentobarbital (50 mg/kg). Heart blood was taken and allowed to sit at room temperature for 2 h. The serum was collected and stored at −4 °C for further experiment. The femurs and major organs (i.e., heart, liver, spleen, lung, and kidney) were taken. All tissues were fixed with 4% paraformaldehyde and stored at room temperature for further experiments.

2.6. Tissue staining experiment

The fixed femoral samples were first decalcified for 2 weeks and then dehydrated with 50%, 70%, 80%, 95%, and 100% alcohol. The treated bone was coated with wax and cut into 10-μm slices for staining by ultramicrotome (Leica, Germany). Some slices were stained by toluidine

blue using a commercial kit. Other slices were used to detect the expression of type II collagen by immumohistochemical staining. Then, hematoxylin and eosin (H&E) staining and toluidine blue staining were performed. TdT-mediated dUTP nick-end labeling (TUNEL) was used to test the apoptosis of the cells. Images were analyzed using an Olympus CX31 light microscope and a confocal laser scanning microscope (Nikon A1, JAPAN).

2.7. Cytokine detection

Interleukin 1β (IL-1β) and tumor necrosis factor-α (TNF-α) contents in the serum were determined by enzyme-linked immunosorbent assay (ELISA) according to the manufacturer's instruction. In this experiment, 10 μl of the serum was diluted five times with PBS, and the 20-μl diluted serum was added to the bottom of the enzyme-labeled plate hole. Then, standard enzyme reagents were added and incubated at 37 °C for 20 min. Cells were washed with detergent five times. The chromogenic agent was added, and the subsequent reaction was set for 10 min at 37 °C. The reaction was stopped by adding the stop solution (the blue color immediately turns to yellow at this time) and was set to zero with the blank hole. The absorbance at each hole was measured sequentially at a wavelength of 450 nm. The absorbance measurement should be conducted within 15 min after adding the stop solution. The cytokine content in the serum was calculated according to the standard curve.

2.8. AuNPs internalized by chondrocytes and macrophages

Raw264.7 and third-generation chondrocytes were seeded in a six-well plate. When 80%–90% of the cells are at the bottom of the plate, cells were scraped off with a scraper. The cells were divided into two parts. One part was fixed with 2.5% glutaraldehyde in phosphate buffer (pH 7.3) at 4 °C for 24 h. Then, cells were fixed with 1% OsO4 for 90 min and finally stained with 1% uranyl acetate at 4 °C for 1 h. After rinsing, the sample was dehydrated in ethanol solution (30%, 50%, 70%, 80%, 90%, and 95% for dehydration series). The resulting cells were embedded in epoxy resin, which was polymerized at 60 °C for 2 days. A thin section with a thickness of 70–90 nm was sliced for TEM analysis using an ultramicrotome (Leica). The thin section was placed on a TEM grid and stained with 2% uranyl acetate and Reynolds lead citrate before taking the image. TEM images were taken using a transmission electron microscope (JEM-2200FS) with an accelerating voltage of 200 kV. The other part was counted with a flow cytometer. Cells were digested with hydrogen peroxide, followed by AuNP digestion with nitrohydrochloric acid. After acid removal, Au atomic content was determined by inductively coupled plasma mass spectrometry (Thermo Fisher Scientific).

2.9. Statistical analyses

Data are represented as the mean ± SD. One-way analysis of variance was conducted to determine the significant differences among different groups. SPSS 19.0 was used to (ns, no significant difference; *$p < 0.05$; **$p < 0.01$; ***$p < 0.001$).

3. Results

3.1. Characterization of AuNPs

Plain AuNPs are fabricated from HAuCl4 reduced by sodium citrate as previously described [38,39] (Fig. 1A). The UV–Vis absorption peak appeared at 520 nm, which is the typical surface plasma absorption peak of AuNPs. The half-peak width was not widened, indicating that the synthesized AuNPs could disperse stably in pure water [40] (Fig. 1B). Indeed, the scanning electron microscopy image indicated that plain AuNPs were monodispersed spherically with a true particle size of 15.8 ± 2.3 nm (Fig. 1C and D). The hydrodynamic diameter was 21.00 ± 2.42 nm (Fig. S1), and the zeta potential was −32.05 ± 1.77 (Fig. 1E). However, the citrate was coated on the surface of plain AuNPs in the form of electrostatic adsorption, and the AuNPs were not colloidally stable when they encounter a positive charge (Fig. 1F). Hence, 11-MUA was used to replace the citrate on the surface of the AuNPs via the formation of Au–S to increase the stability of AuNPs in the physiological environment [41]. The typical surface plasma absorption peaks, monodispersion, and diameter of the modified AuNPs did not change significantly. The surface composition of AuNPs was characterized by X-ray photoelectron spectroscopy. The electron-binding energy spectra of Au showed that the bimodal binding energies of Au in plain AuNPs stabilized by electrostatic adsorption were Au 4F 7/2 (approximately 83.8eV) and Au 4F 5/2 (approximately 87.6eV), respectively, which were smaller than those of Au in modified AuNPs, indicating that the Au atoms of plain AuNPs lost electrons and formed covalent bonds [42] (Fig. 1 G). Moreover, the electron-binding energy spectrum of S was observed. Two kinds of S-binding peaks are found on the surface of modified AuNP samples. According to the standard map, the two pair peaks were Au–S and C–S binding peaks, respectively (Fig. 1H), while there was no S peak on the surface of plain AuNP samples (Fig. S2). These data indicated that MUA had formed an Au–S bond with AuNPs. The basic characteristics of modified AuNPs, such as the morphology, diameter, and zeta potential, were not significantly different from plain AuNPs. However, modified AuNPs can exist stably in the physiological solution (Fig. 1E). Therefore, the modified AuNPs were used for further experiments.

3.2. Cytocompatibility of AuNPs

In previous studies, AuNPs at a concentration of 3 μg/mL executed specific biological functions without toxicity to tumor cells [39] and macrophages [38]. The cytocompatibility of AuNPs at a concentration of 3 μg/mL was measured in chondrocytes as well as macrophages within the joints that are susceptible to AuNPs [43]. Primary chondrocytes were extracted from 5-week-old mice and incubated with AuNPs for 24 h in the second generation. The morphology of chondrocytes was observed under a light microscope with or without toluidine blue staining. Images show that some AuNPs are adsorbed on the surface of chondrocytes, but this did not change the morphology of the chondrocytes (Fig. 2A and B). As a therapeutic agent, AuNPs should be taken up chondrocytes. Therefore, bio-TEM was used to observe sections of macrophage and chondrocytes after AuNP exposure. TEM images reveal that AuNPs are mainly distributed in intracellular vesicles approaching the nucleus from the cell membrane, which indicates that AuNPs can enter chondrocytes through endocytosis, and some of them can escape from the vesicles and enter the cytoplasm (Fig. 2C). Interestingly, significantly more AuNPs entered chondrocytes than macrophages. Indeed, after 24 h of exposure to AuNPs, 15.74 ± 1.00 pg/cell of AuNPs entered chondrocytes, but only 0.85 ± 0.05 pg/cell of AuNPs go into the macrophages as measured by inductively coupled plasma mass spectrometry (Fig. 2D). Then, the cytotoxicity of AuNPs at 3 μg/mL was evaluated in terms of cell survival rate, apoptosis rate, and cell viability.

First, chondrocyte death was determined by calcein–AM/PI double staining kit. Compared with the control group, the number of red fluorescent spots representing dead cells did not increase in the AuNP-treated chondrocyte or macrophage samples, indicating that 3 μg/mL AuNPs is a non-lethal dose to chondrocytes (Fig. 2E). Second, the viability of chondrocytes was measured by CCK-8 kit. The results showed that the metabolic activity (cell viability index) of chondrocytes in the AuNP group was significantly higher than that in the control group, indicating that AuNPs enhance the activity of chondrocytes (Fig. 2F). Third, the apoptosis rate was measured with annexin V–FITC/PI kit. Flow cytometry data showed that AuNP exposure for 24 h did not induce significant cell apoptosis compared with the control group (Fig. 2G). The possible reason is that cartilage tissues consist only of chondrocytes and their secreted ECM, given the important effect of the secretion function of chondrocytes in cartilage tissues. Hence, excluding

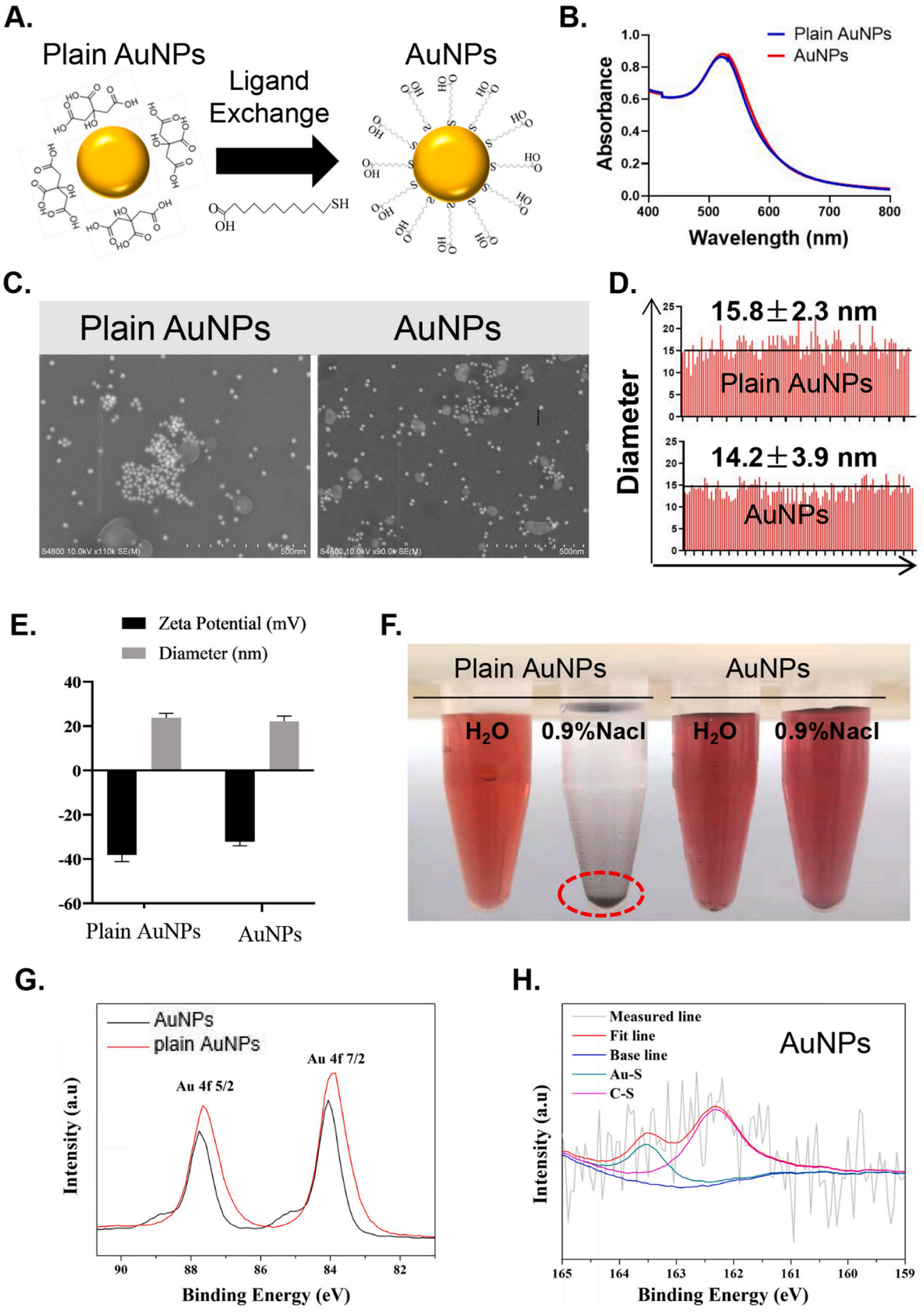

Fig. 1. Synthesis and characterization of gold nanoparticles (AuNPs). A. Modification of plain AuNPs with MUA. B. Ultraviolet–visible absorption spectra of plain AuNPs and AuNPs. C. Representative scanning electron microscopy image of plain AuNPs and AuNPs. D. Particle size of plain AuNPs and AuNPs measured by electron microscopy. E. Zeta potential and hydrodynamic diameter of plain AuNPs and AuNPs determined by dynamic light scattering. F. Modification of AuNPs prevents them from aggregating in both saline (0.9% NaCl) and water (H2O) solutions. G. Electron-binding energy spectra of Au in plain AuNPs and AuNPs. H. Electron-binding energy spectra of S in AuNPs.

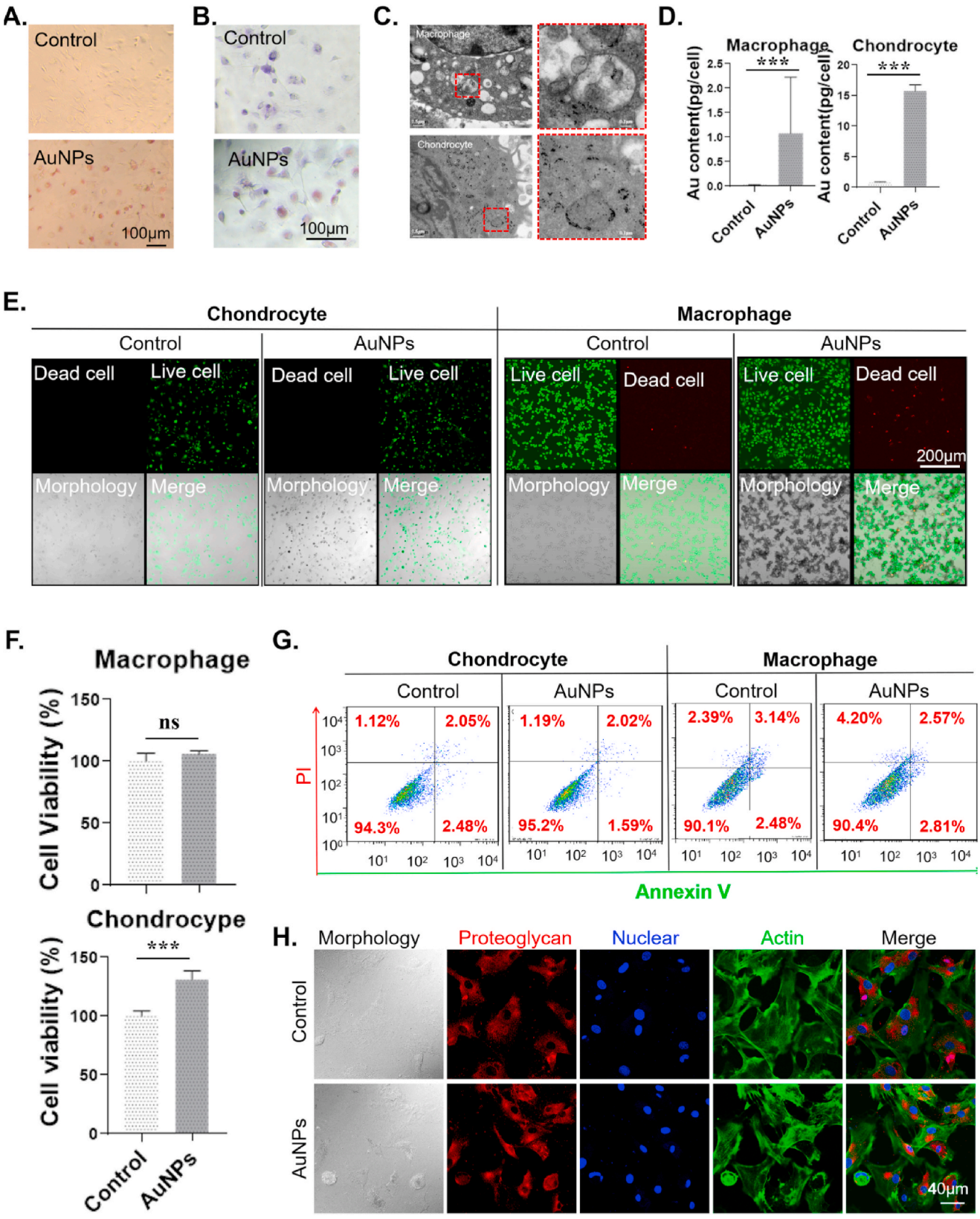

Fig. 2. Cytocompatibility determination of gold nanoparticles (AuNPs). A. Morphology of chondrocytes with or without AuNP exposure. B. Toluidine blue staining of chondrocytes. C. Representative transmission electron microscopy image of the AuNPs (scale bar = 500 nm) taken by macrophages and chondrocytes. D. AuNPs taken up macrophages and chondrocytes as measured by inductively coupled plasma mass spectrometry. E. Live/dead cell double staining after AuNP treatment; dead and living cells stained red and green, respectively. F. Cell viability after the treatment of AuNPs at a concentration of 3 μg/ml for 24 h as measured by Cell Counting Kit-8. G. Flow cytometry was used to determine the apoptosis ratio of macrophages and chondrocytes. H. The expression level of proteoglycans in chondrocytes was measured by immunofluorescence; red fluorescence indicates proteoglycan stained by IgG (H + L) at Dylight 594, green fluorescence represents actin stained by phalloidin at FITC, and blue fluorescence represents the nuclei stained by 4′,6-diamidino-2-phenylindole.

the basic cytotoxicity indicators, the alteration of the secretion functions of chondrocytes caused by AuNPs as therapeutic agents also needs to be avoided. Finally, the effect of AuNPs on chondrocyte function was determined by detecting the expression of proteoglycan, which is an ECM synthesis biomarker [44]. The results indicated that AuNP treatment did not influence the expression level of proteoglycans (Fig. 2H, Fig. S2). Therefore, 3 μg/mL was selected as a possible effective concentration for follow-up experiments.

3.3. AuNPs protect chondrocyte from inflammatory toxicity in vitro

The experiment of AuNPs protecting chondrocytes from inflammation was verified by a model of chondrocyte inflammation induced by LPS. No significant change in the mortality rate and morphology was found among the three groups of chondrocytes (Fig. 3A and B). Interestingly, the viability of chondrocytes was increased significantly in the LPS and LPS + AuNP groups compared with the control group (Fig. 3C). Conversely, LPS significantly increased the apoptosis rate of chondrocytes. AuNPs can significantly alleviate this inflammation-induced damage (Fig. 3D). The expression of proteoglycan in response to LPS treatment was strongly attenuated. However, when added with AuNPs, LPS did not exhibit its ability to reduce the expression of chondrocyte proteoglycan. Compared with the patchy distribution in the control group, proteoglycans in the LPS group showed a spotty and dispersed distribution. The LPS + AuNP-treated cells mitigated the effect caused by LPS (Fig. 3E). These data suggest that AuNPs can protect chondrocytes from inflammatory damage *in vitro*. Further studies have shown that AuNPs could significantly inhibit the inflammatory response of chondrocytes induced by LPS. Specifically, the LPS group of chondrocytes could release significantly more pro-inflammatory cytokines than the control group, while AuNPs could significantly inhibit the release of LPS-induced pro-inflammatory cytokines (Fig. 3F and G). In addition, AuNPs could significantly inhibit the most important ECM molecule (MMP-9) induced by LPS (Fig. 3H). Interestingly, LPS also induced the increased secretion of cartilage matrix synthesis factor (collagen II) (Fig. 3I). This may be due to the feedback regulation between cartilage matrix synthesis and degradation. However, owing to the quantitative and qualitative deficiencies, this response does not repair the cartilage tissue [45].

3.4. Biocompatibility of AuNPs in vivo

Since AuNPs protected the cartilage from inflammatory toxicity *in vitro*, AuNPs were expected to be used to treat inflammation-induced cartilage damage *in vivo*. Before *in vivo* experiments, the biological toxicity of AuNPs should be verified first. As the most direct indicator of biotoxicity, body weight changes in the mice were recorded throughout the treatment cycle. The results showed no significant difference in the body weight between the control and AuNP groups (Fig. 4A). Another more sensitive toxicological indicator is organ coefficients, which were also measured by the ratio of the organ weight to body weight. The results showed that AuNPs did not cause significant changes in the primary organ coefficient, including the liver, kidneys, spleen, and lungs, compared with the control group (Fig. 4B). NPs entering the biological body will cause a series of stress reactions, in which oxidative stress and inflammatory stress are especially serious [46]. The expressions of the inflammatory response factor, including IL-12, TNF-α, and chemokines-2 (CCL-2), were also measured by quantitative real-time polymerase chain reaction (Q-RT-PCR). AuNP injection caused an increase in the transcriptional level of IL-12 in the liver, kidneys, and lungs (Fig. 4C). AuNPs did not induce a severe inflammatory response. Meanwhile, oxidative stress factors, including superoxide dismutase, nicotinamide adenine dinucleotide phosphate oxidase, and heme oxygenase-1, in the primary organ were measured by Q-RT-PCR. The results indicated that AuNPs did not induce oxidative stress reaction (Fig. 4D). Furthermore, H&E staining of primary organs also suggested that AuNPs did not induce system damage (Fig. 4E). Levels of inflammatory factors in the serum were also determined by ELISA. The contents of both IL-12 and TNF-α were not increased after the injection of AuNPs (Fig. 4F and G). In this study, AuNP treatment did not cause serious systemic toxicity in mice.

3.5. AuNPs protected cartilage from inflammatory toxicity in vivo

The protective effects of AuNPs on cartilage were determined in a mice model of LPS-induced cartilage inflammation. H&E staining of femoral tissue sections showed that the boundary of the GP cartilage was clear in the control group, and chondrocytes were arranged in a columnar structure. In the LPS group, however, different chondrocyte types (both PZ and HZ chondrocytes) are impaired. In the LPS + AuNP group, the morphology of the chondrocytes was similar to that of the control group. Importantly, in the LPS group, there is a clear separation of the proliferative zone (PZ) and hypertrophic zone (HZ), without chondrocytes, in the GP of the femur. However, no such damage was observed in mice in the LPS + AuNP group (Fig. 5A). LPS treatment resulted in a significant increase in GP thickness compared with the control group. However, this phenomenon was not observed in the AuNPs + LPS group (Fig. 5B). The thickness of the PZ was also increased after the LPS and AuNP treatment to prevent this abnormal thickening (Fig. 5C). No significant differences were found in the length of HZ (Fig. 5 D). As a result, the expansion of the GP induced by LPS was caused by a significant increase in the thickness of the PZ. Subsequently, AuNPs prevented the expansion of the GP under LPS treatment because of the maintenance of the normal thickness in the PZ. The reason for the PZ widening can be described from two aspects: LPS promoted the proliferation of chondrocytes, and LPS hindered the differentiation of PZ chondrocytes into HZ chondrocytes.

3.6. AuNPs attenuates inflammation-induced chondrocyte apoptosis and cartilage degradation in vivo

Considering the protective effect of AuNPs on chondrocytes, as shown in Fig. 3 that AuNPs attenuate LPS-induced chondrocyte apoptosis and weakened secretory function, the apoptosis rate of mice chondrocytes was determined by TUNEL. As shown in Fig. 6A, the green fluorescence representing apoptosis in the LPS group was higher than those in the control group and AuNP group. Fortunately, the chondrocyte apoptosis rate in the LPS + AuNP group was lower than that in the LPS group. Statistics show that the number of green fluorescence spots, measured by Image J with the same, in the LPS + AuNP group decreased compared with that in the LPS group and reached a significant level (Fig. 6B). In addition, the ECM of the GP was measured by toluidine blue staining. As shown in the image, some areas between the PZ and HZ in the GP did not stain blue (Fig. 6C). This indicated that LPS can induce chondrocyte apoptosis and block the invasion of new chondrocytes in the PZ, resulting in the absence of chondrocytes and ECM (Fig. 5A). Furthermore, the area and integrated density of staining were measured by Image J. Compared with the control group, and LPS decreased the area and integrated density significantly. AuNP treatment can significantly alleviate this effect. The ratio of the cartilage ECM area to the total GP area was also measured by Image J. The statistical trend of the three treatment groups was the same as the area and integrated density trend (Fig. 6D). In addition, the percentage of the collagen area, density, and ratio of the collagen to the GP area in the AuNP + LPS group were higher than those in the LPS group (Fig. 6E).

3.7. AuNPs maintain the balance of the catabolic and anabolic factors of the ECM in vivo

Normally, the integrity and quantity of the ECM in the cartilage depend on the proper balance of catabolic and anabolic activities in the ECM [47]. Considering that AuNPs can maintain the integrity and

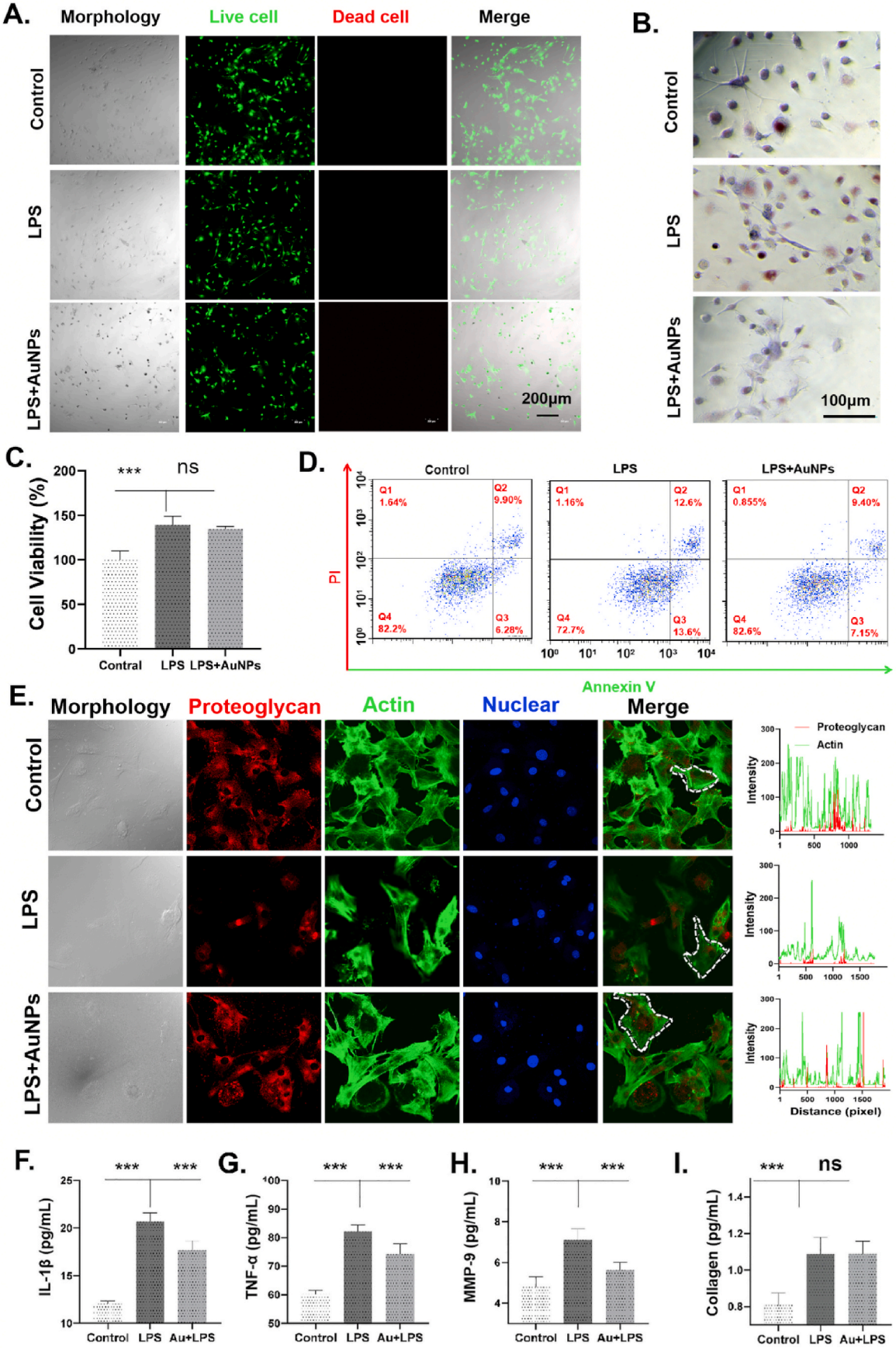

(caption on next page)

Fig. 3. Chondroprotective effects of AuNPs in LPS-induced inflammatory model. A. Live/dead cell double staining; red fluorescence indicated dead cells, and green fluorescence indicated living cells. B. Toluidine blue staining of chondrocytes. C. Cell viability was determined by the Cell Cycle-8 kit. D. Apoptosis ratio of chondrocyte as measured by flow cytometry, including early (Q3) and late (Q2) apoptosis. E. Expression of proteoglycan as measured by immunofluorescence staining: red is proteoglycan, green is actin, and blue is the nuclei. The line profile is the fluorescence distribution of the selected cells in the merged image marked by short white lines, red lines for glycan proteins, and green lines for actin. F and G. Proinflammatory cytokines interleukin 1β (IL-1β) and tumor necrosis factor-α (TNF-α) secreted by chondrocytes were determined by ELISA kit; H and I. Matrix metalloproteinase-9 (MMP) and collagen II secreted by chondrocytes were determined by ELISA kit.

quantity of ECM under inflammation, the molecular turnover rate of ECM was determined by immunofluorescence assay. MMP-9 was regarded as a molecular marker of catabolism because chondrocytes increase their secretions and degrade the ECM in response to inflammatory stress [48]. As shown in Fig. 7A, the MMP-9 content in the GP of LPS-treated mice was significantly increased, which showed that the number, area, and brightness of MMP-9-positive cells were significantly higher than those in the control group. However, these enhanced effects induced by LPS were weakened after AuNP treatment. By contrast, the expression of type II collagen, a molecular indicator of cartilage anabolic activity [49], was significantly lower in the GP of LPS-treated mice than in control mice. The content of type II collagen in the GPs of the AuNP + LPS group was significantly higher than that in the LPS group (Fig. 7B).

4. Discussion

In this study, inflammation caused GP chondrocyte apoptosis and ECM degradation were characterized by a gap between HZ and PZ, which was alleviated after engineered AuNPs treatment. The GP is the developmental center of endochondral ossification (EO). EO is the process by which most mammalian bones, such as the long and short limbs, and some irregular limbs are formed [30]. The GP is always specifically targeted by proinflammatory cytokines to induce chondrocyte apoptosis and cartilage matrix degradation [29]. Inflammation-induced cartilage damage causes fractures when the cartilage is subjected to external force trauma, and growth retardation, deformity, and delayed puberty will occur even in the absence of external force trauma [28]. Because the cartilage is weaker than the bone, GP fractures are common, accounting for 15%–20% of all fractures in children [50]. In addition, up to 56% of children with Crohn's disease, up to 20% of children with cystic fibrosis (CF), and up to 10% of children with ulcerative colitis show symptoms of growth retardation [51]. Delayed puberty has been reported in children with CF, characterized by a lower peak height velocity (PHV) and a growth spurt in late adolescence [52]. The calcification of the GP is insufficient to be seen on an X-ray, as compared to a bone fracture, until signs of healing and new bone formation occur 3–4 weeks after injury. This newly formed bone is called a callus, which leads to the fracture site cannot move the bone back into place.

Although joint replacement is a good treatment for cartilage damage in adults, this excellent strategy is not suitable for GP treatment in children because they are still in the growth stage. Thus, these causes make it more important to protect the cartilage from chronic inflammation caused by various diseases, such as juvenile idiopathic arthritis, CF, ulcerative, Crohn's disease, and inflammatory bowel disease. In this study, LPS, an inflammatory inducer, adversely affects several aspects of chondrogenesis, including chondrocyte apoptosis and cartilage matrix degradation in the GP, and these effects can be ameliorated by AuNP treatment. Through surface self-assembly, AuNPs were carboxylated by MUA so that they could be stably dispersed in normal saline (Fig. 1). The AuNPs can be internalized by chondrocytes without any damage to their morphology, function, or vitality (Fig. 2). In addition to chondrocytes, uptake of AuNPs by macrophages was measured because Au has been reported to accumulate in synovial macrophages surrounding the cartilage tissue in response to inflammatory stress [43]. Interestingly, the intake of AuNPs by chondrocytes was significantly higher than that by macrophages under the same co-incubation condition (Fig. 2C and D). Thus, chondrocytes may be assumed to be the target of these carboxylated AuNPs, which will give the AuNPs a certain targeting ability. Au colloids or salts can play anti-inflammatory roles by down-regulating the expression of proinflammatory factors, which makes them clinically useful in the treatment of arthritis [53,54]. However, the high toxicity and adverse side effects are reasons for the rarity of using Au therapy, also known as cryotherapy, since the 1990s [55]. Fortunately, AuNP-based medicine emerged, which is less toxic and more efficient. Indeed, AuNPs have shown excellent efficacy in arthritis treatment by inhibiting inflammatory response, both as a carrier and as a therapeutic agent, as demonstrated by various studies [56–59]. However, the report about the protective effect of AuNPs on cartilage, especially GP cartilage, as a response to inflammation in children is limited.

LPS is an ideal model to investigate the pathogenesis of inflammation-induced defects because it is a single pathogenic factor and it excludes other influencing factors [60]. As expected, LPS treatment enhanced the viability of chondrocytes to secrete more pro-inflammatory cytokines (Fig. 3F and G) to inhibit the proliferation (Fig. 3A) and increase the apoptosis rate of chondrocytes (Fig. 3D). These common symptoms of cartilage damage caused by either disease-induced inflammation [29] or inflammation alone [61]. Another main pathology of inflammation-induced cartilage damage is the imbalance between anabolic and catabolic molecules (Fig. 3H and I), which results in the inhibition of ECM synthesis, as shown in Fig. 3E. This may be due to the enhanced viability of chondrocytes, indicating chondrocyte activation, through LPS treatment (Fig. 3C) [20]. Encouragingly, none of these pathologic symptoms were observed in the AuNP + LPS group (Fig. 3). All these results indicated that AuNPs can protect the chondrocytes against inflammatory stress *in vitro*. Encouraged by this effect, AuNPs can be used in animals to protect against inflammation-induced GP cartilage damage. Before *in vivo* validation, the physiological toxicity of AuNPs in mice was tested (Fig. 4). When a mouse was exposed to NPs, oxidative and inflammatory stress responses occurred with an increase in inflammatory cytokines in the serum. This will lead to the enlargement of mice organs, destruction of organ structure, and final morphological manifestations of weight loss. Intraperitoneal injection of AuNPs caused a slight increase in IL-12 expression in the liver, kidney, and lung of mice, but no significant effect was noted on the expression of other inflammatory factors or oxidative stress factors in major organs (Fig. 4C and D). Moreover, it even showed an inhibitory effect on the oxidative stress factor HO (Fig. 4D). The slight increase in IL-12 expression in the organs did not cause an increase in the levels of related inflammatory factors in the blood (Fig. 4F and G), and it did not cause damage to the physiological structure of the organs nor did the body weight shows a significant difference (Fig. 4E, B, A).

The orderly arrangement of the GP cartilage cells, forming a columnar structure, can guide bone growth in certain directions to ensure the longitudinal growth of bone-fixed direction [1,30]. Inflammation can impair the arrangement of cartilage cells and will eventually lead to synchronous growth abnormalities growth and (or) GP chondrocytes can cause bone deformities [34]. In our previous study of the LPS-induced bone erosion model, H&E staining not only revealed the altered GP cartilage but also the extended GP thickness, as well as multiple significant fractures at the PZ and HZ junction (Fig. 5). In addition, if LPS promotes chondrocyte proliferation, PZ widening is possible. PZ widening was not caused by the increased chondrocyte proliferation following LPS exposure (Fig. 3). Therefore, it is reasonable to speculate that LPS is induced by inhibiting the differentiation of PZ chondrocytes into HZ chondrocytes to induce further thickening of the

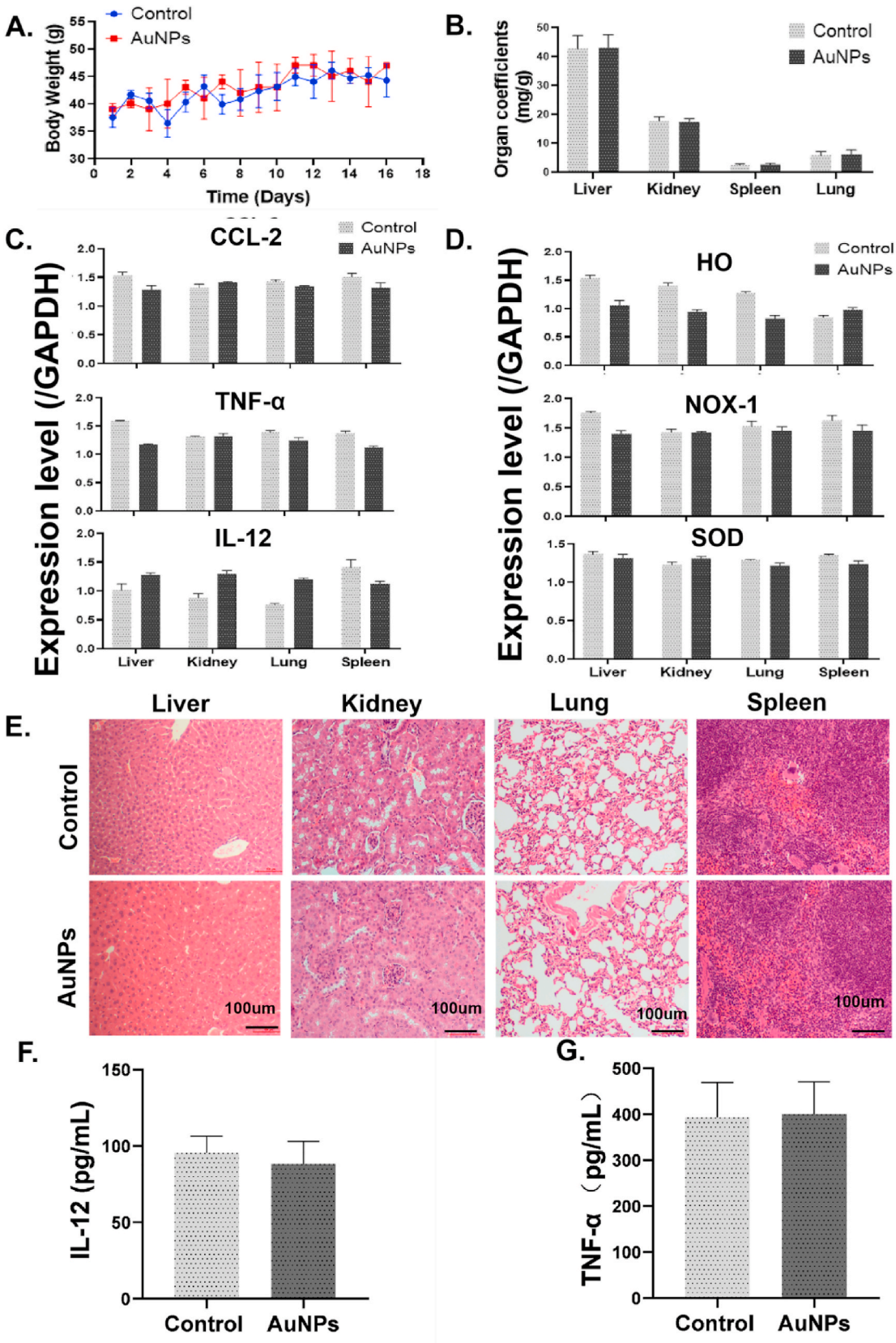

Fig. 4. Biosafety validation of gold nanoparticles *in vivo*. A. Body weight of mice. B. Organ coefficient of mice. C. Expression of inflammatory response factors in the liver, spleen, lungs, and kidney at the transcriptional level. D. Expression of oxidative stress factors in the liver, spleen, lung, and kidneys at the transcriptional level. E. Representative hematoxylin and eosin staining of the liver, spleen, lung, and kidneys. F. Concentration of IL-12 in the serum. G. Concentration of tumor necrosis factor-α in the serum.

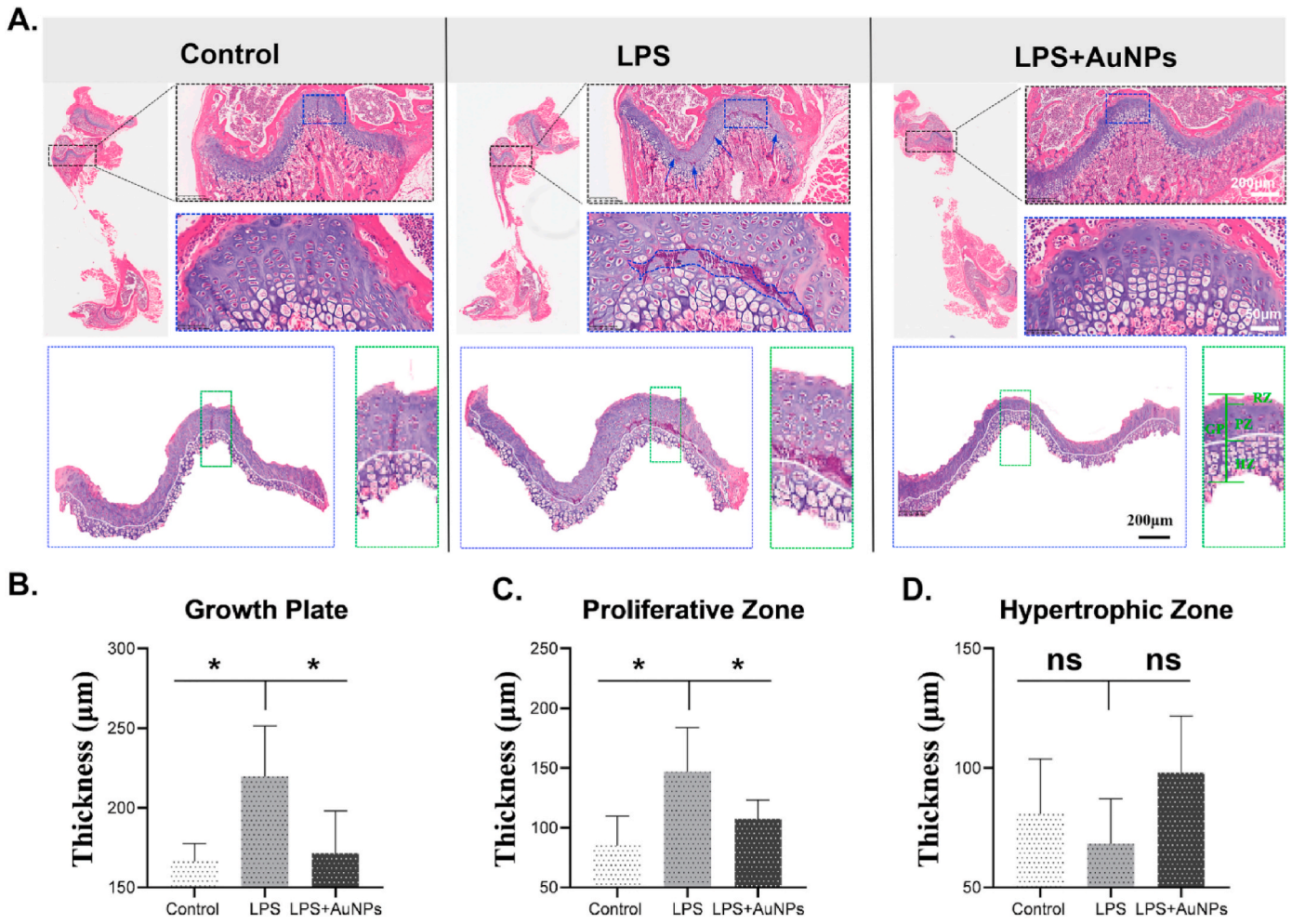

Fig. 5. Protective effect of gold nanoparticles on the growth plate (GP) cartilage in the mouse model of lipopolysaccharide-induced inflammation. A. Representative hematoxylin and eosin staining of GP cartilage on day 16; blue arrow indicates the discontinuous area of the proliferative zone (PZ) and hypertrophic zone (HZ). B–D. Statistics on the thickness of the GP, PZ, and HZ.

PZ, which has also been demonstrated in a previous study [62]. No chondrocytes were present in this fissure, and further toluidine blue staining confirmed the absence of ECM (Fig. 6). None of these pathological features of cartilage damage were present in the AuNP group. PZ and GP extension can be attributed to inflammation interfering with the differentiation of PZ chondrocytes into HZ cells [46]. The gap between HZ and PZ is formed because of the inflammation-induced chondrocyte apoptosis between PZ and HZ, which is in the differentiation stage, and the cell metabolism is more active and sensitive to the LPS-induced inflammatory response, leading to the apoptosis of chondrocytes, which lead to the absence of ECM around the apoptotic chondrocytes. Further studies have exhibited that LPS-induced GP damage showed a significant decrease in the collagen content in the GP in addition to HZ and PZ separation caused by chondrocyte apoptosis. The same reduction of collagen was not observed in the AuNP group (Fig. 6C and D). Presently, the mechanism behind inflammation-induced cartilage degeneration is widely believed to be due to the imbalance between anabolism and catabolism [63,64]. The imbalance between anabolic and catabolic factors has led to the downregulation of type II collagen, aggrecan, and upregulation of MMP-9, MMP-13, and thrombospondin type I motif, member 5 (ADAMTS-5) [65–67], which has been demonstrated in this study (Fig. 7). As it takes >100 years to rebuild the collagen network in cartilage tissues [6,47], it is reasonable to conclude that AuNPs maintain the integrity and quantity of the ECM under inflammation by maintaining the anabolic and catabolic balance of cartilage tissues rather than promoting cartilage regeneration. This indicated that AuNPs can keep the normal development of the GP under inflammatory conditions by preventing inflammatory response instead of cartilage regeneration after the injured.

5. Conclusions

In this study, LPS treatment destroys the GP cartilage, and AuNPs prevented this injury by inhibiting chondrocyte apoptosis and keeping the balance of anabolic and catabolic factors in the ECM. Carboxylated AuNPs, which were stabilized by surface self-assembly, can be internalized by the chondrocytes and inhibit the LPS-induced inflammatory responses in chondrocytes, including decreased chondrocyte proliferation, increased chondrocyte apoptosis, and decreased protein secretion from the chondrocytes. This protective effect of AuNPs on chondrocytes can maintain the accurate arrangement of GP chondrocytes, chondrocyte activity, expression, and integrity of the ECM in the context of inflammation. Further investigation on the specific mechanism of AuNPs targeting chondrocytes and their metabolic pathways *in vivo* is necessary to improve the protective effect of AuNPs on the cartilage under inflammatory conditions. The chondroprotective property of AuNPs in combination with other drugs can help in the treatment of inflammation-related cartilage diseases.

Credit author statement

Xue Bai: Conceptualization, Methodology, Writing – original draft.

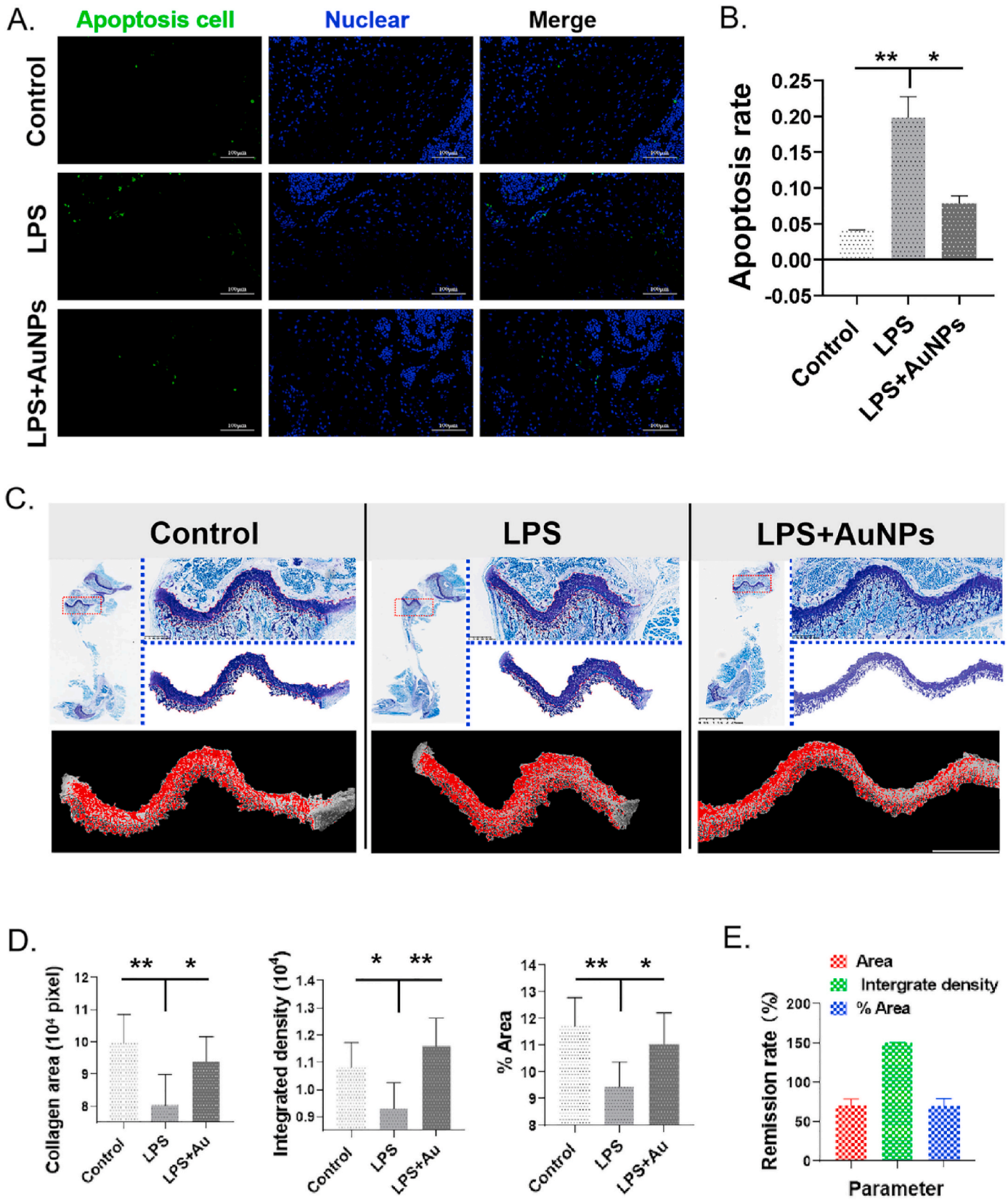

Fig. 6. Effect of AuNPs on the inflammation-induced chondrocyte apoptosis and cartilage degradation. A. Representative images for the chondrocyte apoptosis analysis by TUNEL staining. The green influence signal represents the apoptotic cell, and the blue influence signal represents all cells. B. Apoptosis rate of chondrocytes measured by the number of apoptotic chondrocytes versus the total number of chondrocytes. C. Toluidine blue staining of the cartilage ECM, which can be stained dark blue. D. The histograms from left to right represent the collagen area, integrated density, and ratio of the collagen area to the total GP area stained by toluidine blue staining. E. The proportions of the collagen area, density, and ratio of collagen to the GP area in the AuNP + LPS group were higher than those in the LPS group.

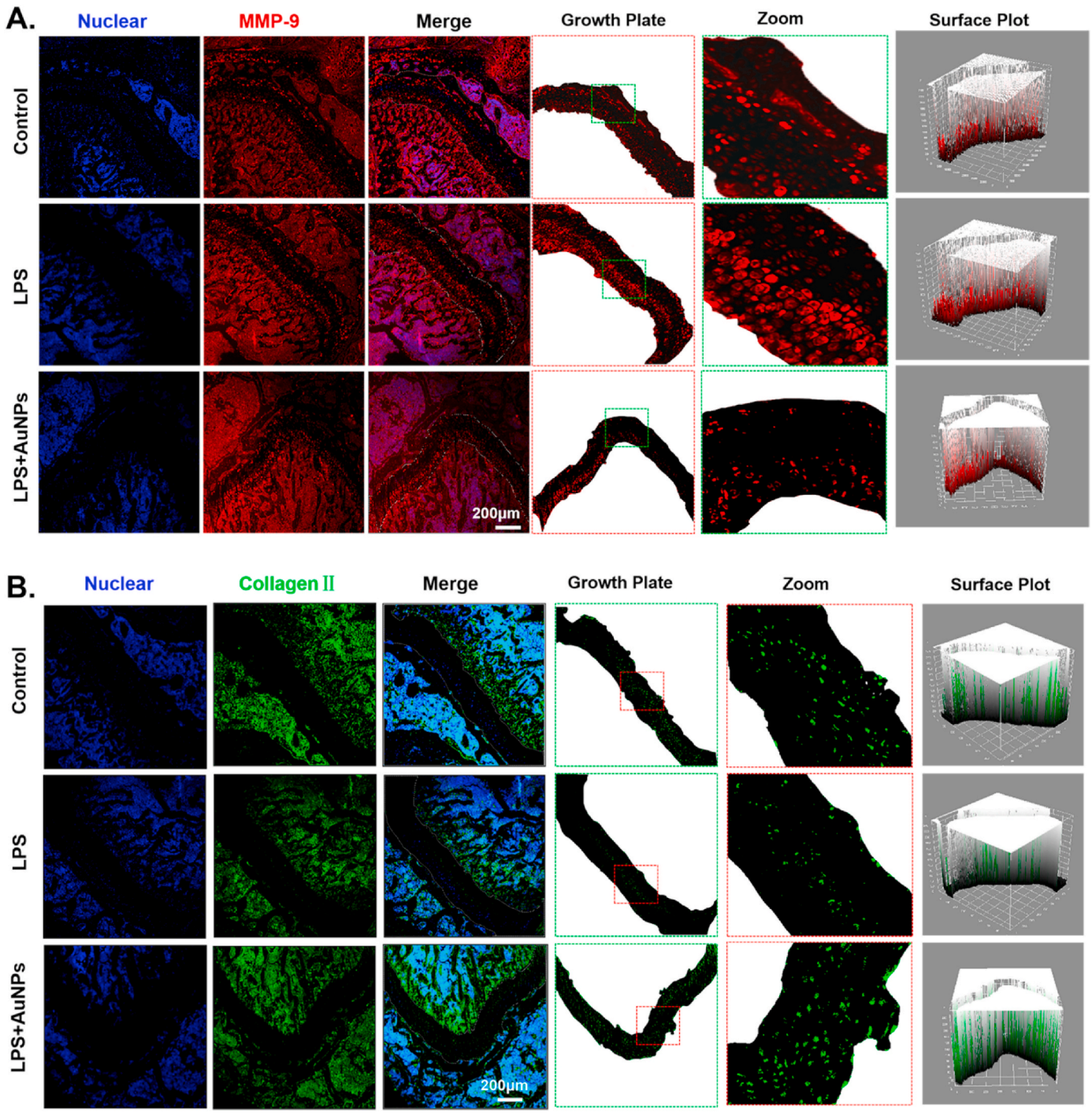

Fig. 7. Effect of gold nanoparticles on the turnover of extracellular matrix molecules. A. Representative image of MMP-9 immunofluorescence staining of the growth plate cartilage. The small figure on the left represents the fluorescence intensity, and distribution was analyzed by a surface plot. B. Representative image of type II collagen immunofluorescence staining of the growth plate cartilage. The small figure on the left represents the fluorescence intensity, and distribution was analyzed by a surface plot.

Hongyan Sun: **Lina Jia** and **Bo Chen**: Methodology, Data curation Investigation. **Junjie Xu** and **Peng Zhang**: Writing – review & editing, Validation. **Yu Gu**: Funding acquisition. **Lin Feng** and **Deyuan Zhang**: Supervision and Resources.

Declaration of competing interest

The authors declare that they have no known competing financial interests or personal relationships that could have appeared to influence the work reported in this paper.

Data availability

Data will be made available on request.

Acknowledgments

This research was funded by Beijing Municipal Fund for

Distinguished Young Scholars (Grand No. JQ22022).

Appendix A. Supplementary data

Supplementary data to this article can be found online at https://doi.org/10.1016/j.mtbio.2023.100795.

References

[1] D. Umlauf, S. Frank, T. Pap, J. Bertrand, Cell. Mol. Life Sci. 67 (24) (2010) 4197, https://doi.org/10.1007/s00018-010-0498-0.
[2] C.A. McDevitt, J. Marcelino, Sports Med. Arthrosc. Rev. 2 (1) (1994) 1.
[3] J. Eschweiler, N. Horn, B. Rath, M. Betsch, A. Baroncini, M. Tingart, F. Migliorini, Life 11 (4) (2021) 302.
[4] P. Morouço, C. Fernandes, W. Lattanzi, J. Funct. Biomater. 12 (1) (2021) 17.
[5] K.M. Heinemeier, P. Schjerling, J. Heinemeier, S.P. Magnusson, M. Kjaer, Faseb. J. 27 (5) (2013) 2074, https://doi.org/10.1096/fj.12-225599.
[6] K.M. Heinemeier, P. Schjerling, J. Heinemeier, M.B. Møller, M.R. Krogsgaard, T. Grum-Schwensen, M.M. Petersen, M. Kjaer, Sci. Transl. Med. 8 (346) (2016) 346ra90, https://doi.org/10.1126/scitranslmed.aad8335.
[7] M.P. Murphy, L.S. Koepke, M.T. Lopez, X. Tong, T.H. Ambrosi, G.S. Gulati, O. Marecic, Y. Wang, R.C. Ransom, M.Y. Hoover, H. Steininger, L. Zhao, M. P. Walkiewicz, N. Quarto, B. Levi, D.C. Wan, I.L. Weissman, S.B. Goodman, F. Yang, M.T. Longaker, C.K.F. Chan, Nat. Med. 26 (10) (2020) 1583, https://doi.org/10.1038/s41591-020-1013-2.
[8] Z. Man, X. Hu, Z. Liu, H. Huang, Q. Meng, X. Zhang, L. Dai, J. Zhang, X. Fu, X. Duan, C. Zhou, Y. Ao, Biomaterials 108 (2016) 157, https://doi.org/10.1016/j.biomaterials.2016.09.002.
[9] H. Rogan, F. Ilagan, X. Tong, C.R. Chu, F. Yang, Biomaterials 228 (2020), 119579, https://doi.org/10.1016/j.biomaterials.2019.119579.
[10] X. Xu, Y. Liang, X. Li, K. Ouyang, M. Wang, T. Cao, W. Li, J. Liu, J. Xiong, B. Li, J. Xia, D. Wang, L. Duan, Biomaterials 269 (2021), 120539, https://doi.org/10.1016/j.biomaterials.2020.120539.
[11] J.S. Temenoff, A.G. Mikos, Biomaterials 21 (5) (2000) 431, https://doi.org/10.1016/S0142-9612(99)00213-6.
[12] A.R. Martín, J.M. Patel, H.M. Zlotnick, J.L. Carey, R.L. Mauck, npj Regen. Med. 4 (1) (2019) 12, https://doi.org/10.1038/s41536-019-0074-7.
[13] P.T. Newton, L. Li, B. Zhou, C. Schweingruber, M. Hovorakova, M. Xie, X. Sun, L. Sandhow, A.V. Artemov, E. Ivashkin, S. Suter, V. Dyachuk, M. El Shahawy, A. Gritli-Linde, T. Bouderlique, J. Petersen, A. Mollbrink, J. Lundeberg, G. Enikolopov, H. Qian, K. Fried, M. Kasper, E. Hedlund, I. Adameyko, L. Sävendahl, A.S. Chagin, Nature 567 (7747) (2019) 234, https://doi.org/10.1038/s41586-019-0989-6.
[14] K. Mizuhashi, W. Ono, Y. Matsushita, N. Sakagami, A. Takahashi, T.L. Saunders, T. Nagasawa, H.M. Kronenberg, N. Ono, Nature 563 (7730) (2018) 254, https://doi.org/10.1038/s41586-018-0662-5.
[15] M.-F. Hsueh, P. Önnerfjord, M.P. Bolognesi, M.E. Easley, V.B. Kraus, Sci. Adv. 5 (10) (2019), eaax3203, https://doi.org/10.1126/sciadv.aax3203.
[16] W.W. Curl, J. Krome, E.S. Gordon, J. Rushing, B.P. Smith, G.G. Poehling, Arthrosc. J. Arthrosc. Relat. Surg. 13 (4) (1997) 456, https://doi.org/10.1016/S0749-8063(97)90124-9.
[17] W. Widuchowski, J. Widuchowski, T. Trzaska, Knee 14 (3) (2007) 177, https://doi.org/10.1016/j.knee.2007.02.001.
[18] J.M. Llovet, J. Zucman-Rossi, E. Pikarsky, B. Sangro, M. Schwartz, M. Sherman, G. Gores, Nat. Rev. Dis. Prim. 2 (1) (2016), 16018, https://doi.org/10.1038/nrdp.2016.18.
[19] H. Takeda, T. Nakagawa, K. Nakamura, L. Engebretsen, Br. J. Sports Med. 45 (4) (2011) 304, https://doi.org/10.1136/bjsm.2010.082321.
[20] H.E. Jasin, J. Clin. Invest. 72 (6) (1983) 2014, https://doi.org/10.1172/JCI111166.
[21] H.S. Hwang, H.A. Kim, Int. J. Mol. Sci. 16 (11) (2015), 26035.
[22] J.-P. Pelletier, J. Martel-Pelletier, S.B. Abramson, Arthritis Rheum. 44 (6) (2001) 1237, https://doi.org/10.1002/1529-0131(200106)44:6<1237::AID-ART214>3.0.CO;2-F.
[23] M.S. Kocher, R. Tucker, T.J. Ganley, J.M. Flynn, Am. J. Sports Med. 34 (7) (2006) 1181, https://doi.org/10.1177/0363546506290127.
[24] J.A. Buckwalter, Operat. Tech. Orthop. 7 (4) (1997) 263, https://doi.org/10.1016/S1048-6666(97)80028-6.
[25] J.P. Cezard, G. Touati, C. Alberti, J.P. Hugot, C. Brinon, P. Czernichow, Horm. Res. 58 (Suppl 1) (2002) 11, https://doi.org/10.1159/000064759.
[26] H. Ji, A. Pettit, K. Ohmura, A. ortiz-lopez, V. Duchatelle, C. Degott, E. Gravallese, D. Mathis, C. Benoist, J. Exp. Med. 196 (2002) 77.
[27] S.G. Koniaris, S.E. Fisher, C.T. Rubin, A. Chawla, J. Pediatr. Gastroenterol. Nutr. 25 (2) (1997) 137.
[28] F. Amaro, F. Chiarelli, Biomedicines 8 (11) (2020) 458.
[29] F. Cirillo, P. Lazzeroni, C. Sartori, M.E. Street, Int. J. Mol. Sci. 18 (9) (2017) 1878.
[30] H.M. Kronenberg, Nature 423 (6937) (2003) 332, https://doi.org/10.1038/nature01657.
[31] A. Goulding, Med. Sport Sci. 51 (2007) 102.
[32] I. Jones, S. Williams, N. Dow, A. Goulding, Osteoporos. Int. 13 (2002) 990.
[33] B.S. Kirschner, Acta Paediatr. 79 (s366) (1990) 98, https://doi.org/10.1111/j.1651-2227.1990.tb11608.x.
[34] A.H. Jheon, C. Mitgutsch, Acta Zool. 89 (3) (2008) 277, https://doi.org/10.1111/j.1463-6395.2007.00316.x.
[35] F. Burdan, J. Szumiło, A. Korobowicz, R. Farooquee, S. Patel, A. Patel, A. Dave, M. Szumiło, M. Solecki, R. Klepacz, J. Dudka, Folia Histochem. Cytobiol. 47 (1) (2009) 5, https://doi.org/10.2478/v10042-009-0007-1.
[36] M. Alini, Y. Matsui, G.R. Dodge, A.R. Poole, Calcif. Tissue Int. 50 (4) (1992) 327, https://doi.org/10.1007/BF00301630.
[37] H.-P. Gerber, T.H. Vu, A.M. Ryan, J. Kowalski, Z. Werb, N. Ferrara, Nat. Med. 5 (6) (1999) 623, https://doi.org/10.1038/9467.
[38] X. Bai, Y. Gao, M. Zhang, Y.-n. Chang, K. Chen, J. Li, J. Zhang, Y. Liang, J. Kong, Y. Wang, W. Liang, G. Xing, W. Li, G. Xing, Nanoscale 12 (6) (2020) 3871, https://doi.org/10.1039/C9NR09698A.
[39] X. Bai, J. Zhang, Y.N. Chang, W. Gu, G. Xing, Int. J. Mol. Sci. 19 (9) (2018) 2790.
[40] X. Liu, M. Atwater, J. Wang, Q. Huo, Colloids Surf. B Biointerfaces 58 (1) (2007) 3.
[41] H. Häkkinen, Nat. Chem. 4 (6) (2012) 443, https://doi.org/10.1038/nchem.1352.
[42] J. Radnik, C. Mohr, P. Claus, Phys. Chem. Chem. Phys. 5 (1) (2003) 172, https://doi.org/10.1039/B207290D.
[43] B. Vernon-Roberts, J.L. Dore, J.D. Jessop, W.J. Henderson, Ann. Rheum. Dis. 35 (6) (1976) 477, https://doi.org/10.1136/ard.35.6.477.
[44] C.B. Knudson, W. Knudson, Semin. Cell Dev. Biol. 12 (2) (2001) 69, https://doi.org/10.1006/scdb.2000.0243.
[45] M.B. Mueller, R.S. Tuan, PM&R 3 (6, Supplement) (2011) S3, https://doi.org/10.1016/j.pmrj.2011.05.009.
[46] E. Fireman, J. Asthma 49 (1) (2012) 8, https://doi.org/10.3109/02770903.2011.641047.
[47] M.B. Goldring, K.B. Marcu, Arthritis Res. Ther. 11 (3) (2009) 224, https://doi.org/10.1186/ar2592.
[48] P.S. Burrage, K.S. Mix, C.E. Brinckerhoff, Front. Biosci. Landmark 11 (1) (2006) 529, https://doi.org/10.2741/1817.
[49] G. Chiara, C. Ranieri, Curr. Pharmaceut. Des. 15 (12) (2009) 1334, https://doi.org/10.2174/138161209787846739.
[50] F. Shapiro, Chapter 7 - epiphyseal growth plate fracture–separations, in: F. Shapiro (Ed.), Pediatric Orthopedic Deformities, Academic Press, San Diego, 2001, p. 519.
[51] B.P. Abraham, S. Mehta, H.B. El-Serag, J. Clin. Gastroenterol. 46 (7) (2012) 581, https://doi.org/10.1097/MCG.0b013e318247c32f.
[52] M. Bournez, G. Bellis, F. Huet, Arch. Dis. Child. 97 (8) (2012) 714, https://doi.org/10.1136/archdischild-2011-301069.
[53] S.L. Schepens, A.L. Kratz, S.L. Murphy, J. Gerontol.: Series A 67 (10) (2012) 1114, https://doi.org/10.1093/gerona/gls076.
[54] K.S. Santangelo, G.J. Nuovo, A.L. Bertone, Osteoarthritis Cartilage 20 (12) (2012) 1610, https://doi.org/10.1016/j.joca.2012.08.011.
[55] A. Balfourier, J. Kolosnjaj-Tabi, N. Luciani, F. Carn, F. Gazeau, Proc. Natl. Acad. Sci. USA 117 (37) (2020), 22639, https://doi.org/10.1073/pnas.2007285117.
[56] W.N.S. Campos, V.S. Marangoni, D.A. Sonego, M.A. Andrade, E.M. Colodel, R.L. de Souza, Osteoarthritis Cartilage 23 (2015) A397, https://doi.org/10.1016/j.joca.2015.02.732.
[57] C. Cutler, J. Lattimer, J. Kelsey, M. Kuchuk, D. Oconnor, S. Bal, K. Katti, J. Nucl. Med. 56 (supplement 3) (2015) 363.
[58] H. Lee, M.-Y. Lee, S.H. Bhang, B.-S. Kim, Y.S. Kim, J.H. Ju, K.S. Kim, S.K. Hahn, ACS Nano 8 (5) (2014) 4790, https://doi.org/10.1021/nn500685h.
[59] L. Leonavičienė, G. Kirdaitė, R. Bradūnaitė, D. Vaitkienė, A. Vasiliauskas, D. Zabulytė, A. Ramanavičienė, A. Ramanavičius, T. Ašmenavičius, Z. Mackiewicz, Medicina 48 (2) (2012) 16.
[60] C.N. Serhan, J. Savill, Nat. Immunol. 6 (12) (2005) 1191, https://doi.org/10.1038/ni1276.
[61] K. Mårtensson, D. Chrysis, L. Sävendahl, J. Bone Miner. Res. 19 (11) (2004) 1805, https://doi.org/10.1359/JBMR.040805.
[62] X. Cheng, P.-Z. Li, G. Wang, Y. Yan, K. Li, B. Brand-Saberi, X. Yang, J. Cell. Physiol. 234 (3) (2019) 2593, https://doi.org/10.1002/jcp.27025.
[63] S.S. Glasson, R. Askew, B. Sheppard, B. Carito, T. Blanchet, H.-L. Ma, C.R. Flannery, D. Peluso, K. Kanki, Z. Yang, M.K. Majumdar, E.A. Morris, Nature 446 (7131) (2007) 102, https://doi.org/10.1038/nature05640.
[64] K. Li, Y. Zhang, Y. Zhang, W. Jiang, J. Shen, S. Xu, D. Cai, J. Shen, B. Huang, M. Li, Q. Song, Y. Jiang, A. Liu, X. Bai, Ann. Rheum. Dis. 77 (6) (2018) 935, https://doi.org/10.1136/annrheumdis-2017-212658.
[65] F. Echtermeyer, J. Bertrand, R. Dreier, I. Meinecke, K. Neugebauer, M. Fuerst, Y. J. Lee, Y.W. Song, C. Herzog, G. Theilmeier, T. Pap, Nat. Med. 15 (9) (2009) 1072, https://doi.org/10.1038/nm.1998.
[66] D. Miao, X. Bai, D.K. Panda, A.C. Karaplis, D. Goltzman, M.D. McKee, Bone 34 (4) (2004) 638, https://doi.org/10.1016/j.bone.2003.12.015.
[67] Y. Zhang, F. Vasheghani, Y. Li, M. Blati, S. Kayla, H. Fahmi, B. Lussier, J. P. Pelletier, J. Martel-Pelletier, M. Kapoor, Osteoarthritis Cartilage 22 (2014) S340, https://doi.org/10.1016/j.joca.2014.02.631.